Simple Box Model for Modeling Future Arctic Sea Ice Thickness at Different Latitudes

Jonatan Haraldsson
haral080@umn.edu
jonhara@chalmers.se

Alex Monteil
monte427@umn.edu

Abstract

We have used a simple box model based on vertical heat transport to simulate the thickness of Arctic sea ice in the future at different latitudes. In essence, the model used for ice thickness was based on previous work by M.J McGuinness, where our addition was to add latitude dependence, seasonal variations and an average increase in global mean temperature (GMT) to the surface-air temperature [1]. The ice albedo feedback was modeled with albedo as a function of ice thickness. With albedo feedback, surface-air temperatures were modeled using Budyko's equation, seen in class. From this, two different simulations, with and without ice-albedo feedback, were run, and both gave maximum ice thickness values of 2.5 m and 3.8 m respectively. Furthermore, with an average increase in global mean temperature (GMT) of 0.73 °C per decade, the simulations without albedo feedback predict that the Arctic sea will be ice free in 55 years. Using the same GMT increase, and adding observational data, the simulation with albedo feedback predicts the first ice-free summer by 2040.

May 1st 2025
Course: *Introduction to Mathematical Climate Models*
Course Code: *MATH 5421*

University of Minnesota
Twin Cities, MN, USA

Contents

1 Introduction

Earth's global mean temperature (GMT) has been increasing at an alarming rate, which might profoundly change the world we live in [2]. Nowhere on Earth is it clearer than in the Arctic regions, where the ice-covered landscapes are gradually disappearing. With data collected since 1979, there is a significant difference when comparing the extent of the ice in September $1979-2000$ to September $2000-2023$, as done in Figure 1 [3]. To illustrate, the mean extent of sea ice in September $1979-2000$ was $6.9 \times 10^6\,\mathrm{km}^2$ compared to $5.0 \times 10^6\,\mathrm{km}^2$ in September $2000-2023$, which is a decrease in size by $25\,\%$. Moreover, recent reports suggest that the maximum Arctic sea ice extent of 2025, reached on March 22$^{\text{nd}}$ 2025, was the lowest annual maxima recorded [4]. However, loss of sea ice will most certainly have consequences far beyond the Arctic regions. For instance, greater open-sea surface area means greater absorption of solar radiation, leading to the well-known ice-albedo feedback mechanism, which might further increase air temperatures. In addition, there are reports suggesting that less ice in the Arctic may cause a collapse of the Atlantic Meridional Overturning Circulation (AMOC), a system of ocean currents crucial for making northern Europe experience comfortable temperatures [5]. In summary, scientific models describing sea ice dynamics are important in trying to understand the climate across the globe, and they are crucial when making future predictions.

Historically, one of the earlier models for describing the dynamics of a boundary with different phases (e.g. ice and water or ice and air) was the Stefan Problem, named after the Slovenian physicist Jožef Stefan [6]. Over the years, models for describing sea ice growth have been further developed, and current models often have both a dynamic part, described by the equations of motion, and a thermodynamic part, described by heat fluxes and heat conduction through the ice [7]. For this project, due to limited time and experience handling partial differential equations, a simple one-dimensional model was used to find sea ice thickness at different latitudes, and make a future projection inline with the current rise in GMT.

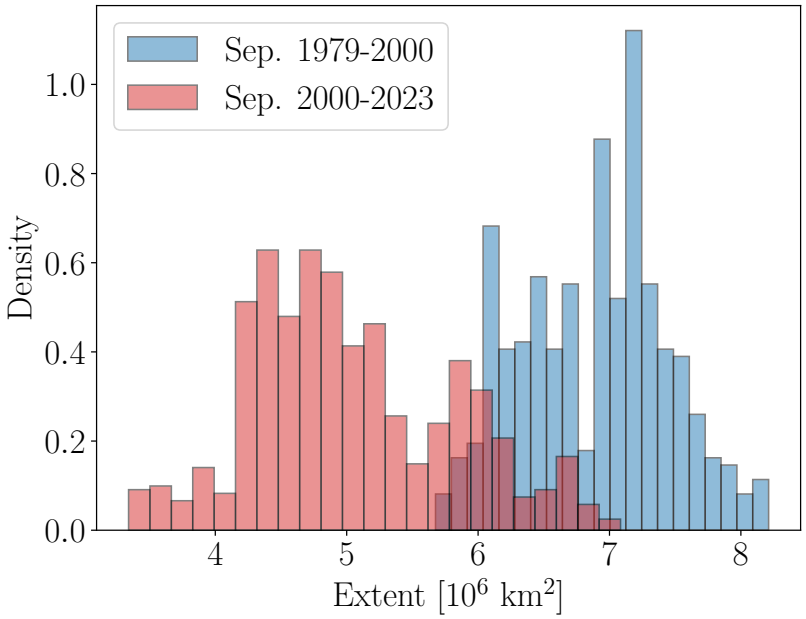

Figure 1: Histogram, made in `Python` over two time intervals of sea ice extent in September [3]. The blue histogram covers the period from 1979 to 2000, while the red histogram covers the period from 2000 to 2023. The height of the bins are given in normalized counts, density.

2 Theory, Sea Ice

This section gives a brief theoretical introduction to sensible and latent heat, different heat fluxes, oceanic transport and the albedo-feedback mechanism.

2.1 Thermodynamics basics

Sensible heat is defined as heat which causes a thermodynamic system to change in temperature when it is added or removed from the system. On the other hand, latent heat is defined as heat, which does not cause a thermodynamic system to change in temperature when it is added or removed from the system. Instead, it is absorbed or released by the system as part of a phase transition.

2.2 Atmospheric Heat Flux

Atmospheric heat flux refers to the rate of heat energy transfer between the Earth's surface and the atmosphere primarily through the movement of air and water vapor molecules. In the context of arctic sea ice, it contributes to heat transfer at the ice-air boundary layer.

2.3 Oceanic Heat Flux

Oceanic heat flux refers to the rate of heat energy transfer between the ocean and arctic sea ice at the boundary layer. This phenomenon occurs through turbulent mixing in the ocean's upper layer, vertical diffusion of heat from the deeper ocean layer and oceanic transport. It contributes to heat transfer at the ice-water boundary layer.

2.4 Oceanic Transport

Oceanic transport refers to the movement of water, heat, salt, and momentum by large-scale ocean circulation systems. It occurs through:

- Advection: the movement of water masses carrying heat and salinity due to the wind, Earth's Coriolis effect, and difference in density in the medium due to salinity changes often referred to as thermohaline circulation.
- Diffusion: heat and salt gradually spread from warmer to cooler regions.
- Turbulent mixing: shear, wind-stress causing ice drift and buoyancy differences causing heat convection.

2.5 Albedo-Feedback Mechanism

Albedo refers to the proportion of solar radiation reflected by a surface. Snow reflects between 80 and 90 percent of solar radiation [8], sea ice between 60 and 80 percent [9] and the open ocean between 5 and 7 percent [10].

Albedo creates a feedback loop in which warming leads to ice melting which causes melt ponds on the ice surface. These melt ponds expose dark ocean water which has reduced albedo. In turn, more solar radiation is absorbed which means more heat, accelerating the melting process in a self amplifying behavior. However, the opposite is true for snow-covered ice sheets, since snow has a high albedo.

3 Method

Ice dynamics in terms of growth or melt are directly related to both atmospheric heat flux and oceanic heat flux. As a result, the modeling approach selected is driven from the first principles of physics. It is a box model focusing on the thermodynamics at the ice-air boundary and at the ice-water boundary. This model is expressed as a dynamical system.

In this section, an expression for sea ice growth rate is derived using a similar approach as [1] and [11]. Next, a function for surface air temperature was formulated to include different latitudes, seasonal variations, and a future GMT increase. In addition, an attempt to model the ice-albedo feedback was also made. Lastly, the equations were solved numerically using `Python` with and without the ice-albedo feedback. For coding, the following libraries `NumPy`, `Matplotlib`, `Pandas` were used, and syntax errors were solved using library documentation and the use of search engines.

3.1 Deriving an Expression for Sea Ice Growth Rate

To begin, consider the simple set-up given in Figure 2, consisting of three regions: air ($z < 0$), ice ($0 < z < h$), and ocean ($z > h$). Furthermore, the temperature at the air-ice boundary is $T(z = 0) = T_a$, while $T(z = h) = T_o$ denotes the temperature at the ocean-air interface. According to the second law of thermodynamics, heat flows from hot to cold, and thus heat flows through the ice sheet whenever $T_a \neq T_o$. Mathematically, the vertical heat flux q for this system is given by Fourier's law

$$q = -k\frac{\mathrm{d}T}{\mathrm{d}z}, \tag{1}$$

where $k = 2.2\,\mathrm{W\,m^{-1}\,{}^{\circ}C^{-1}}$ the thermal conductivity of ice, T is the temperature, and z the depth [12].

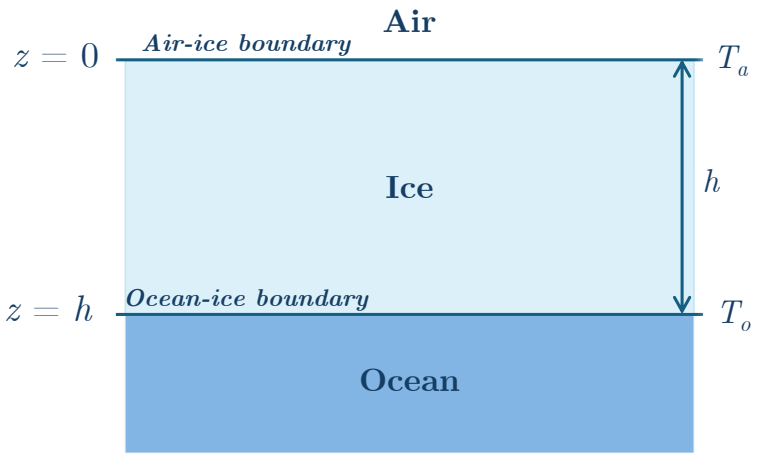

Figure 2: Schematic illustration of an ice sheet of thickness h with an upper boundary at $z = 0$ facing air and a lower boundary at $z = h$ facing the ocean. The temperatures at the boundaries are $T(0) = T_a$ and $T(h) = T_o$.

Following the work of [1], an expression for the moving ice boundary, $\frac{\mathrm{d}h}{\mathrm{d}t} = \dot{h}$, was found by first assuming that the temperature profile across the ice is linear, which for $T(z = 0) = T_a$ and $T(z = h) = T_o$ gives

$$T(z) = \frac{T_o - T_a}{h}z + T_a \Rightarrow \frac{\mathrm{d}T}{\mathrm{d}z} = \frac{T_o - T_a}{h}. \tag{2}$$

In essence, the heat flux q is directly related to $\dot{h}$ as q is driven by the latent heat released during the phase transition at the moving ice-ocean boundary $z = h(t)$ [1]. More specifically, $q = -\dot{h}\rho L$, where $\rho = 917\,\mathrm{kg\,m^{-3}}$ the density of ice, and $L = 334\,\mathrm{kJ\,kg^{-1}}$ the latent heat of water. By putting Equations 1, 2 together and re-arranging for $\dot{h}$ the expression

$$\dot{h} = \frac{k(T_o - T_a)}{\rho L h} \tag{3}$$

can be used to solve for the ice thickness $h(t)$. As an example, if $T_a < T_o$ heat flows from the warmer ocean to the colder air, thus, $q \overset{\text{Eq.1}}{=} -k(T_o - T_a)/h < 0$, which promotes freezing as $\dot{h} = -q/\rho L > 0$*.

Lastly, an additional term that accounts for the heat flux from the ocean was subtracted from Equation 3. This done by both [1] and [11], giving

$$\dot{h} = \frac{k(T_o - T_a)}{\rho L h} - \frac{Q_o}{\rho L}. \tag{4}$$

The flux term Q_o depends on ocean currents and the temperature of the deep ocean [1].

3.2 Modeling Air Temperatures

To model the thickness of sea ice at different latitudes, T_a was modeled as a function of latitude $\theta_{lat.}$ using

$$\bar{T}_a(\theta_{lat.}) = a + b\left[\frac{3}{2}\cos^3(\theta_{lat.})\left(\frac{2}{3} + \sin^2(\theta_{lat.})\right)\right], \tag{5}$$

where $a \approx -12\,^\circ\mathrm{C}$ and $b \approx 40\,^\circ\mathrm{C}$ [13]. At the ice-ocean boundary, T_o is assumed to be constant at $T_o = -1.8\,^\circ\mathrm{C}$, the freezing temperature of sea ice [1].

To make T_a depend on both seasonal variations and the long-term increase in GMT seen in the Arctic regions, some additional terms were added to $\bar{T}_a(\theta_{lat.})$ in Equation 5 giving

$$\mathcal{T}_a(\theta_{lat.},t) = \underbrace{\bar{T}_a(\theta_{lat.})}_{\text{Annual avg.}} + \underbrace{\widetilde{T}(\theta_{lat.})\sin\left(2\pi t/365 - d_0\right)}_{\text{Seasonal change}} + \underbrace{\delta T \cdot t/365}_{\text{GMT increase}}, \tag{6}$$

where t is given in days, $\widetilde{T}$ is the amplitude of annual temperature variations, $\delta T \approx 0.073\,^\circ\mathrm{C/yr}$ is an average yearly temperature increase [14], and d_0 is some start date. However, as seasonal temperature variations also vary with latitude, $\widetilde{T}$ was modeled accordingly

$$\widetilde{T}(\theta_{lat.}) = (\widetilde{T}_{Arc.} - \widetilde{T}_{Eq.})\sin(\theta_{lat.}) + \widetilde{T}_{Eq.} \tag{7}$$

The temperature variation given by Equation 7 was artificially constructed, and the seasonal temperature variations was chosen to be $\widetilde{T}_{Eq.} \approx 2.5\,^\circ\mathrm{C}$ in the equatorial regions and $\widetilde{T}_{Arc.} \approx 15\,^\circ\mathrm{C}$ in the Arctic regions. To illustrate, $\widetilde{T}(\theta_{lat.})$ is shown in Figure 3.

Note that the signs here are a consequence of the choosing z-direction to be downwards.

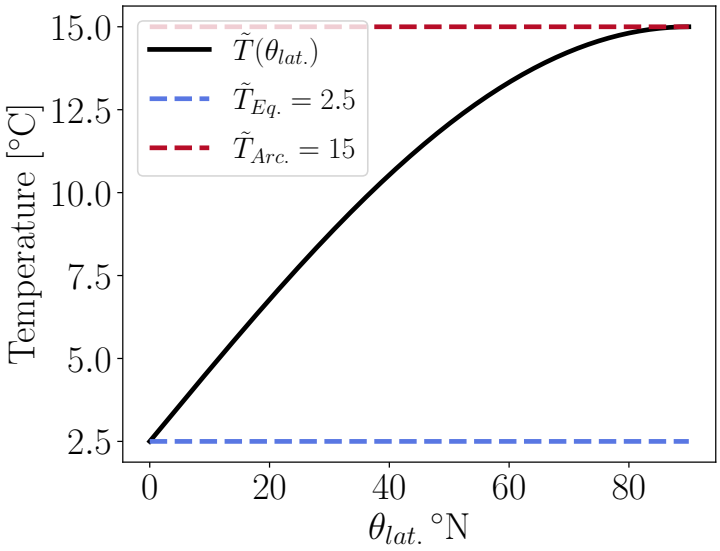

Figure 3: Seasonal temperature variation $\widetilde{T}$ as a function of latitude $\theta_{lat.}$ using Equation 7.

In summary, in the expression for $\mathcal{T}_a(\theta_{lat.},t)$, $\bar{T}_a(\theta_{lat.})$ is used as a baseline, as it somewhat captures the average annual temperature at different latitudes, $\widetilde{T}(\theta_{lat.})$ captures seasonal variations and δT the long-term GMT increase.

3.3 Modeling Oceanic Heat Flux

Modeling the ocean flux (Q_o) is important, as it determines the maximum (equilibrium) sea ice thickness, i.e. $\dot{h} = 0$. Q_o was therefore tuned such that $h(\theta_{lat.})$ matched "real" sea ice thickness data, while still being within reasonable limits. According to [11] Q_o is "a few tens of $\mathrm{W\,m^{-2}}$", and the average maximum thickness far from land was estimated to be in the range $3-4\,\mathrm{m}$ [15].

After some trial-and-error, and under the assumption that Q_o depends on the average surface air temperature ($\bar{T}_a$), the following expression

$$Q_o = \frac{Q_{max} - Q_{min}}{2}(\tanh(\pi f(\bar{T}_a)) + 1) + Q_{min} \tag{8}$$

gave reasonable results for the oceanic heat flux, where $f(\bar{T}_a)$ is a linear function such that $f : [-25\,^\circ\mathrm{C}, 5\,^\circ\mathrm{C}] \to [-1, 1]$, $Q_{min} = 5\,\mathrm{W\,m^{-2}}$ and $Q_{max} = 20\,\mathrm{W\,m^{-2}}$. To clarify, the idea behind Equation 8 is to give a smooth transition from $Q_{min} = 5\,\mathrm{W\,m^{-2}}$ to $Q_{max} = 20\,\mathrm{W\,m^{-2}}$ as the average temperature increase from $-25\,^\circ\mathrm{C}$ to $5\,^\circ\mathrm{C}$.

3.4 Modeling Ice Albedo Feedback

To incorporate ice-albedo feedback in the model, the average annual temperature $\bar{T}_a(\theta_{lat.})$ in Equation 5 was changed to Budyko's heat balance equation shown in class [16]. The equation is given by

$$T^*_\eta(y) = \frac{Qs(y)(1 - \alpha(y,\eta)) - A + C\bar{T}^*_\eta}{B + C}, \tag{9}$$

where $Q = 343$, $A = 202$, $B = 1.9$ and $C = 3.04$ are constants. $s(y) = 1 - 0.241(3y^2 - 1)$ is a latitude distribution function for $y = \sin(\theta_{lat.})$, $\bar{T}_\eta^*$ is the average temperature and η the latitude of the ice line. A detailed breakdown of all terms in the Equation 9 can be found in the lecture slides [16].

A dynamic albedo, in this case albedo as a function of ice thickness, was implemented using the following expression

$$\alpha(\theta_{lat.},\eta) = \frac{\alpha_D(h) - \alpha_1}{2}\left[\tanh(M[\sin(\theta_{lat.}) - \sin(\eta)]) + 1\right] + \alpha_1$$

where $\alpha_D(h) = \alpha_2 - (\alpha_2 - \alpha_1)e^{-\mu h}$ with $\mu = 1.209$ [17]. The use of hyperbolic tangent with parameter $M = 5$ was inspired by [18] as a way to smooth out the discontinuity in T_η^* seen in class. For this project, $\alpha_1 = 0.32$ and $\alpha_2 = 0.62$ as seen in class [16]. In conclusion, the simulations with ice-albedo feedback were using the following expression for air-surface temperature

$$\mathcal{T}_a(\theta_{lat.},t) = \underbrace{T_\eta^*(y(\theta_{lat.}))}_{\text{Annual avg.}} + + \underbrace{\delta T \cdot t/365}_{\text{GMT increase}}. \tag{10}$$

3.5 Numerical Implementation

To model the ice thickness with the time and latitude dependent surface air temperature ($\mathcal{T}_a(\theta_{lat.},t)$), Equation 4 was solved iteratively using

$$h_{n+1} = h_n + \dot{h}_n(t_{n+1} - t_n), \text{ where } \dot{h}_n = \left(\frac{k(T_o - \mathcal{T}_a(\theta_{lat.},t_n))}{\rho L h_n} + \frac{Q_o(\bar{T}_a(\theta_{lat.}))}{\rho L}\right) \tag{11}$$

where n corresponds to one day. Note that the expression for surface temperature, $\mathcal{T}_a(\theta_{lat.},t_n)$, is either given by Equation 6 or 10 depending on if the simulation was run with or without ice-albedo feedback. However, prior to simulation, h and $\dot{h}$ had to be bounded to keep them from reaching non-physical values, e.g. negative h or very large values of $\dot{h}$, as $h \to 0$. This was done by setting $\dot{h} = 0$ if $h \leq 0$, and $\max\{\dot{h}\} = 10\,\text{cm/day}$ [7].

In terms of programming the simulation, Equation 11 was solved iteratively using two loops, one loop over n and one loop over $\theta_{lat.}$, however, their order depended on if the simulation was run with or without albedo feedback. A more efficient approach for the simulations without albedo feedback, was to calculate h_n for all n before moving to the next $\theta_{lat.}$. With albedo feedback, the setup was the opposite, i.e. h_n was calculated for all $\theta_{lat.}$ before moving to $n + 1$. In the case with albedo feedback, the ice line latitude η was also updated for each n by finding the maximum $\theta_{lat.}$ where $h = 0$. With η_n, an estimated total ice sheet area was found using the formula for a spherically symmetric cap

$$A_n = 2\pi R^2(1 - \sin(\eta_n)),$$

where $R = 6378\,\text{km}$ is Earth's radius [19].

To ensure that the thickness reached its equilibrium, Equation 11 was run for 50 years without GMT increase (i.e. $\delta T = 0$ in Equation 6 and 10), starting with $h_0(\theta_{lat.}) = 0$ for evenly spread values of $\theta_{lat.} \in (0°\,\text{N}, 90°\,\text{N})$. In other words, the ice sheets were built up from zero over 50 years. For $t > 50$ years, the GMT term was set to $\delta T = 0.073\,°\text{C/year}$, simulating future scenarios. Lastly, a linear regression was fit to the estimated ice sheet area as it decreases.

4 Results

First, the resulting $h(t)$ without albedo feedback, but with seasonal variations, is given in Figure 4 for four latitudes. From the figure, there is a steady decrease in thickness for $t > 50\,\text{yr}$, especially for the summer thickness, which is predicted to disappear completely after 55 years (see Table 1). Although it is still receding, the winter ice thickness seems to be less sensitive to the added GMT increase. In addition, Table 1 also includes the equilibrium thickness ($h(t = 50)$) during summer and winter for the latitudes studied.

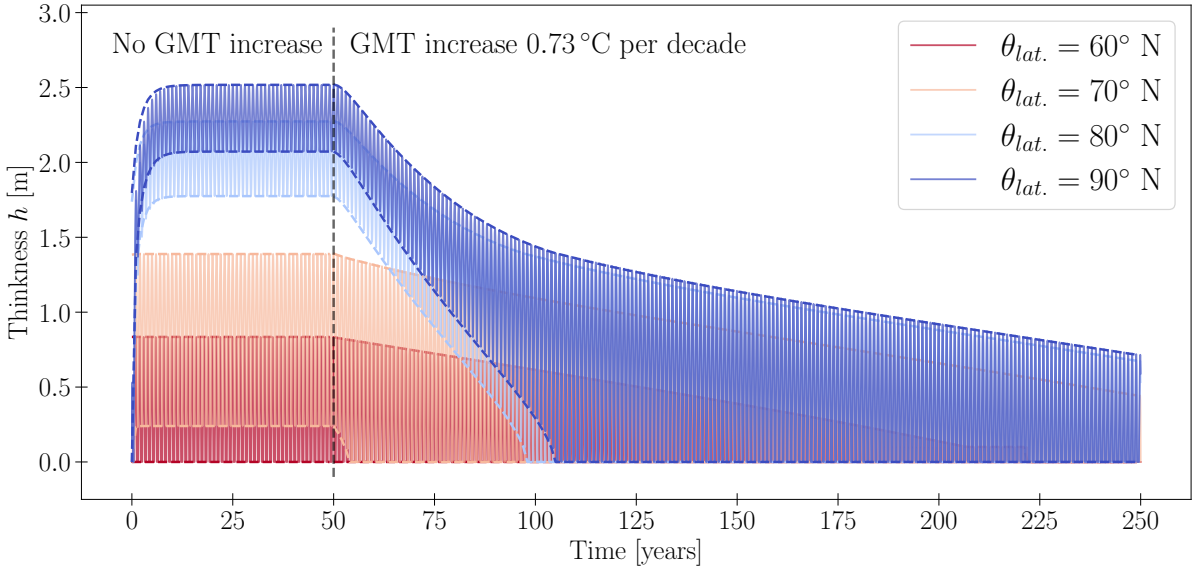

Figure 4: Modeled thickness for four latitudes. For $t < 50\,\text{yr}$, the GMT increase was set to zero and then 0.73 °C per decade for $50\,\text{yr} < t < 250\,\text{yr}$.

Table 1: Years to an ice-free September and March for different latitudes with GMT increase of 0.73 °C per decade, and the maximum/minimum ice thickness for $t = 50$ years.

Latitude	**Years to no summer ice**	**Years to no winter ice**	$\boldsymbol{h_{max}}$ $\boldsymbol{t = 50}$	$\boldsymbol{h_{min}}$ $\boldsymbol{t = 50}$
60° N	0	172	0.83 m	0.00 m
70° N	4	284	1.39 m	0.24 m
80° N	48	338	2.27 m	1.77 m
90° N	55	348	2.52 m	2.07 m

Second, $h(t)$ with albedo feedback, but without seasonal variations, is given in Figure 5 for all simulated latitudes, however, 60° N, 70° N, 80° N,and 90° N were highlighted. In this case, there is no ice growth for $\theta_{lat.} < 68.5°$ N, which gives $\eta = 68.5°$ N and an ice sheet area of $17.1 \times 10^6\,\text{km}^2$. In addition, when ice albedo feedback is included the simulation seems to give slightly higher maximum thickness values (see Table 2). For $t > 50$, there also is a steady decrease in sea ice thickness. Lastly, this simulation suggests that $h = 0$ for $t > 117 - 50 = 67\,\text{yr}$ (Table 2) for 90° N.

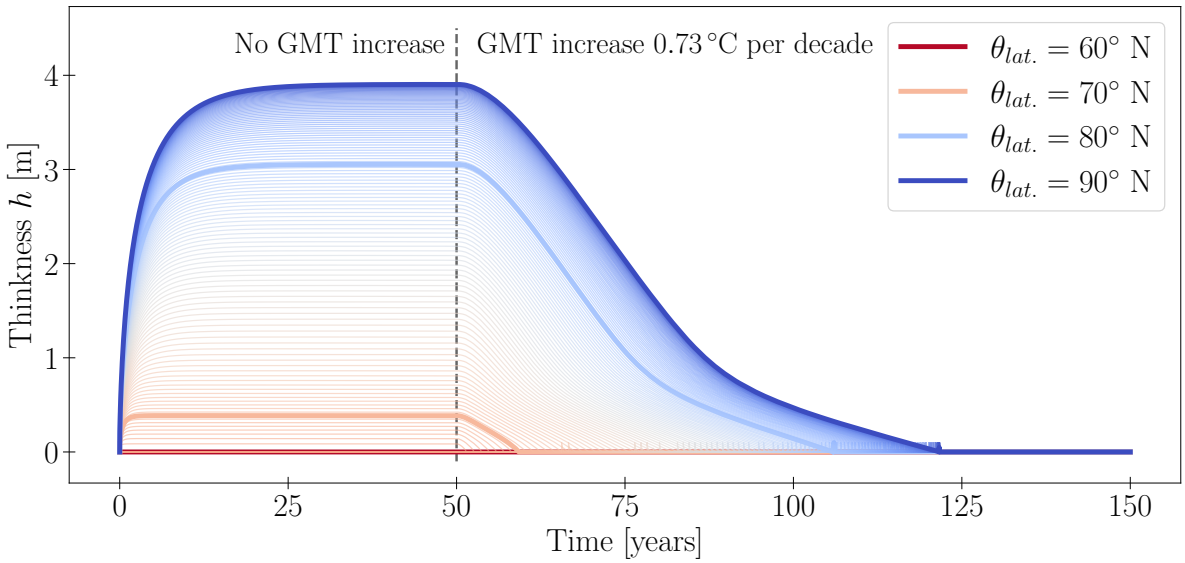

Figure 5: Modeled thickness for four latitudes. For $t < 50\,\text{yr}$, the GMT increase was set to zero and then 0.73 °C per decade for $50\,\text{yr} < t < 150\,\text{yr}$.

Table 2: Years to an ice-free Arctic for different latitudes with GMT increase of 0.73 °C per decade, and the maximum ice thickness for $t = 50$ years.

Latitude	**Years to no ice**	$\boldsymbol{h_{max}(t = 50)}$
60° N	0	0
70° N	8	0.39
80° N	56	3.05
90° N	67	3.90

Third, the estimated ice sheet area ($A(t_n)$) at each iteration is given in Figure 6, together with a linear fit. For reference, actual data for mean sea ice extent during March and September for different year intervals are also included in the figure [3]. The linear fit for the time interval with decreasing sea ice, was found to be $\hat{A}(x) = -0.259x + 17.14$, where x is years after $t = 50$ and $\hat{A}$ in millions km^2. Using the linear fit with the mean from March 2023 (14.44×10^6 km^2) as offset predicts that it takes $x = 14.44/0.259 \approx 56$ years to melt all sea ice. This will, according to this model, happen in $2023 + 56 = 2079$. Similarly, using the mean for September 2023 (4.37×10^6 km^2) as offset predicts that it takes $x = 4.37/0.259 \approx 17$ years to reach the first ice free summer. This will, according to this simulation, happen in $2023 + 17 = 2040$.

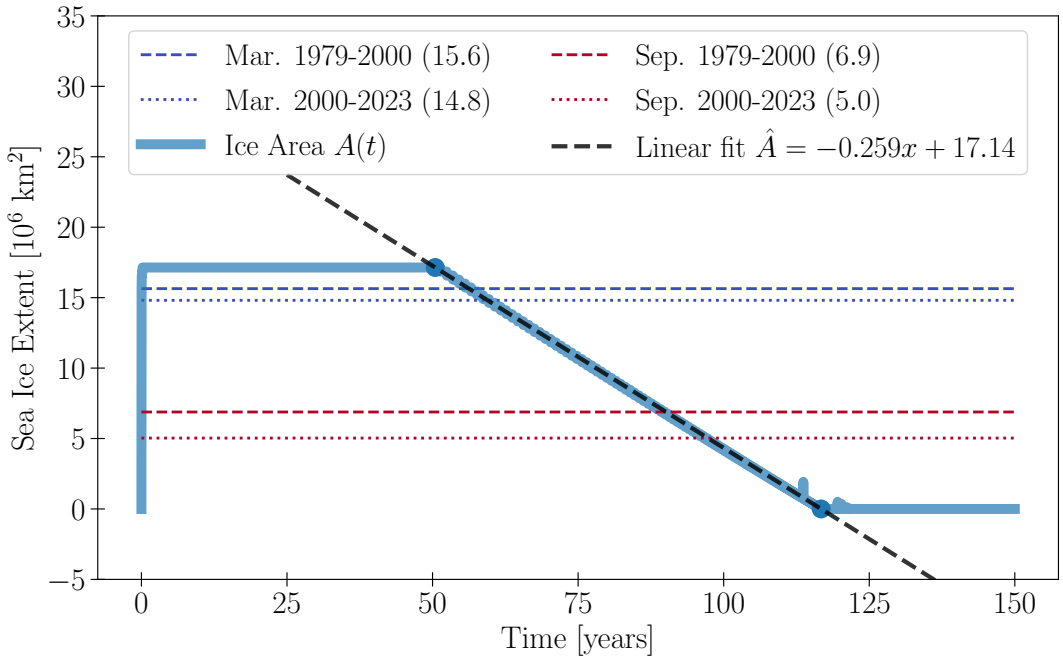

Figure 6: Sea ice area with albedo feedback, along with a linear fit for the decreasing region, and actual data for mean sea ice extent in March and September for different year intervals. The ice extent for the year intervals are given in parenthesis.

5 Discussion

In this section, the results from the two simulations are discussed and compared to data from more sophisticated models. In addition, some of the assumptions and models limitations are discussed along with some future outlook.

5.1 Simulation Results and Comparison to Other Models

The simulations based on the model gave satisfactory results with respect to real-world observed data, which suggests that it captures some important drivers of sea ice dynamics. For both simulations, the results show a latitudinal dependence for the ice thickness with thickness increasing with latitude, i.e. thickest ice at the poles and thinner towards the equator. The simulation without albedo, (Figure 4) suggests that some sea ice forms during winter at latitude 60° N, while the second simulation (Figure 5) suggests no ice growth for latitudes below 68.5° N.

The first 50 years of the simulation are meant to closely match the ice built up over the past and from year 50 onward the simulation shows what we can expect from present day conditions all the way to 250 years from now in the first simulation and all the way to 150 years from now in the second.

With the albedo included, the total ice sheet area was estimated to be $17.1 \times 10^6\,\text{km}^2$, which is rather close to the mean in March (1979-2000) of $15.64 \times 10^6\,\text{km}^2$, however, not too close to the annual mean of $11.9 \times 10^6\,\text{km}^2$ in the same period [3]. Furthermore, the linear fit suggests a yearly sea ice area decrease of $\sim 2.59 \times 10^5\,\text{km}^2/\text{yr}$, which is significantly higher than the decline of $0.79 \times 10^5\,\text{km}^2/\text{yr}$ seen for September from 1979 to 2022 [20]. However,

when comparing to more sophisticated models, some suggest that the Arctic may be ice free by $\sim$ 2050, which is just a decade later than 2040 using our slope [20], [21]. For this to happen in 2050, the melting of sea ice has to be accelerated, which highlights that sea ice melting may not be linear after all.

For the first case, without albedo, comparing year 50 to 2023, the model predicts a mean thickness of $\sim$ 0.8 m at 70° N, $\sim$ 2 m at 80° N and $\sim$ 2.3 m at 90° N, those figures are reasonably close to recent observed data but are on the conservative side as some sources show lower figures for mean ice thickness at those latitudes [22]. As time progresses, the simulation predicts the first ice-free summers at latitude 80° N near 2075. It also shows near-loss of multi-year ice at latitude 90° N around 2080. These results are consistent with intermediate emissions scenarios (SSP2-4.5) of IPCC predictions which use CMIP6 models [23]. Overall, the model seems to display consistent latitudinal dependence for ice thickness, satisfactory baseline thickness near observed data for recent years and a realistic poleward retreat of the ice line as the GMT increases.

5.2 Assumptions and Model Limitations

In its current form, the model simplifies sea ice growth and melt to thermodynamics at the boundary layers. However, it does not account for the dynamic part meaning the influence of forces applied to sea ice. In effect, sea ice is acted upon by many force-carrying phenomena involving stress such as the wind, the oceanic transport, the Coriolis effect, the Ekman transport and the internal ice stress [24]. More advanced models could also account for melt ponds, which drastically speeds up the melting due to the albedo-feedback mechanism, or snow cover on top of the ice, which has the opposite effect.

Further assumptions were made, such as keeping the ocean layer temperature at the water-ice boundary (T_o) constant at $-1.8\,^{\circ}\mathrm{C}$, and reducing the oceanic heat flux to one term. These are also assumptions that do not account for all parameters that are part of the oceanic transport and the oceanic heat flux at the ice-water boundary layer. However, those factors were deliberately ignored in favor of a simpler model intended to look at a more easily-interpretable, lower-resolution, and longer-term picture of the future of Arctic sea ice.

Among other limitations, we note that the model in its current form does not involve a direct physical coupling between sea-ice thickness and air and ocean temperatures within the dynamical system. A fully coupled physical model would involve a system of partial differential equations relating the rate of change in ice thickness, to the rate of change in air temperature, the rate of change in upper ocean layer temperature and the rate of change of salinity at the mixed layer.

As a final note, we assumed a linear temperature profile through the ice. However, in reality, the temperature distribution across sea ice $T(z,t)$ depends on both z and time t, e.g. it takes time before a change in the upper temperature (T_a) propagates through the ice. To investigate this assumption, the heat equation was solved for the system (see Appendix A). $T(z,t)$ converges to a linear profile after $\sim$ 20 days, which means that the linear assumption might be a valid simplification when looking at more long-term ice growth.

5.3 Future Outlook for the Model

One of the more important future implementations that should be considered is trying to combine seasonal variations and albedo feedback. Combining the two in the current model

made it highly sensitive to small temperature variations and the seasonal temperature variations had to be excluded. Furthermore, exploring different expressions for the GMT-increase function, to somewhat mimic different climate scenarios, might also be interesting.

Although this would be more computationally intensive, another addition to the model is to account for longitudinal differences in sea ice growth in the Arctic caused by ocean currents. This could be done by adding a longitudinal dependence to the oceanic heat flux (Q_o) and the surface air temperature ($\mathcal{T}_a(\theta_{lat.},t)$), and then solving Equation 11 with another loop over all longitudes.

Finally, some further considerations include having a fully physically coupled dynamical system relating the rates of change of surface air temperature and upper ocean layer temperature to the rate of change of ice thickness. Such a model could take the following form

$$\begin{cases} \frac{\partial h}{\partial t} = \frac{k(T_o - T_a)}{\rho L h} \\ \frac{\partial T_a}{\partial t} = \frac{1}{R_a}\left(Qs(y)(1 + s_1(y)\cos(\frac{2\pi}{\tau}t)(1 - \alpha(T_a)) - A - BT_a + C(\bar{T_a} - T_a)\right) \\ \frac{\partial T_o}{\partial t} = \frac{1}{R_o}(Q_{in} - Q_{out}), \end{cases}$$

where the first expresses sea ice growth, the second is Budyko's heat balance equation [16], and the third is oceanic heat balance.

- $T_a(y,t)$: surface air temperature at latitude y and time t
- R_a: Effective heat capacity of the air-surface layer
- Q, A, B, C: Average solar radiation constant, parameters of linear approximation of outgoing longwave radiation and heat transport parameter (horizontal diffusion) from Budyko
- $s(y)$: Normalized annual insolation distribution
- $s_1(y)$: Latitude-dependent seasonal modulation amplitude
- τ: Period of one year in seconds
- $\alpha(T_a)$: Temperature-dependent albedo as a sigmoid function inspired by [25]
- $\bar{T_a}(t)$: Global average surface temperature
- R_o: Heat capacity of ocean layer
- $Q_{in} - Q_{out}$ heat flux difference

Above, $\frac{\partial T_o}{\partial t}$ is a generalized form for the sources and sinks of heat affecting the temperature of the upper-oceanic layer but a formal expression for it could be formulated from scientific literature such as [26][27][28][29] in order to complete the model. Such a dynamical model can be solved numerically by converting the partial differential equation system into a discretized ordinary differential equation system which is then solved using a numerical method of choice such as the Runge-Kutta algorithm. This was done as a proof-of-concept for $\frac{\partial T_a}{\partial t}$.

6 Conclusion

In conclusion, the model used in this report, despite its simplicity, displays satisfactory accuracy in describing sea-ice thickness at different latitudes and at predicting its future evolution under a global mean temperature increase. The simulations that included albedo feedback suggest a completely ice-free Arctic sea by 2079, and the first ice-free summer by 2040. The simulations without albedo offer more conservative figures suggesting the first ice-free summer will happen within 55 years. Compared to more sophisticated models within the scientific community, the simulations with albedo gave reasonably close results, which indicates that the overall trends are captured by our model. However, improvements, such as combining seasonal variations, albedo feedback and exploring different expressions for GMT increase, might provide better accuracy. Nonetheless, the predictions offered by this simple box model are indeed concerning with the first ice-free summer predicted to occur in 2040, only 15 years may be separating us from a climate disaster and the potential for extinction of numerous Arctic species.

As a final note, we think this project was a great addition to the lecture content offered throughout this class, as it gave us the opportunity to apply some of the concepts as well as expand upon them by reading additional scientific literature to inform our modeling decisions. We both feel like we have learned a lot about the driving factors behind sea ice dynamics and their impact on Earth's eco-systems. Lastly, let's hope we as a species can recognize the severity of the problem and start treating it as a global priority.

References

[1] M. Mcguinness, "Modelling sea ice growth," *The ANZIAM Journal*, vol. 50, pp. 306–319, Jan. 2009. DOI: 10.1017/S1446181109000029.

[2] NOAA, National Centers for Environmental information. "Climate at a glance: Global time series." (2025), [Online]. Available: https://www.ncei.noaa.gov/access/monitoring/climate-at-a-glance/global/time-series (visited on 04/05/2025).

[3] Fetterer, F.; Knowles K.; Meier W.; Savoie M.; Windnagel A., *Sea ice index, version 3*, en, 2017. DOI: 10.7265/N5K072F8. [Online]. Available: https://nsidc.org/data/G02135/versions/3.

[4] M. Scott. "2025 winter maximum sea ice extent in arctic smallest on record," NOAA, National Centers for Environmental information. (Apr. 9, 2025), [Online]. Available: https://www.climate.gov/news-features/event-tracker/2025-winter-maximum-sea-ice-extent-arctic-smallest-record#:~:text=Despite%20the%20late%20peak%2C%20it,heart%20of%20the%20Arctic%20Ocean. (visited on 04/13/2025).

[5] J. Meyer. "Thinner arctic sea ice may affect the AMOC," University of Gothenburg. (Mar. 31, 2025), [Online]. Available: https://www.gu.se/en/news/thinner-arctic-sea-ice-may-affect-the-amoc (visited on 04/20/2025).

[6] Wikipedia. "Stefan problem." (Jan. 14, 2025), [Online]. Available: https://en.wikipedia.org/wiki/Stefan_problem (visited on 03/04/2025).

[7] O. M. Johannessen, L. P. Bobylev, E. V. Shalina, and S. Sandven, "Sea ice modelling," in *Sea Ice in the Arctic*. Springer, Cham, 2019, ch. 8, ISBN: 978-3-030-21301-5. DOI: 10.1007/978-3-030-21301-5. [Online]. Available: https://link.springer.com/book/10.1007/978-3-030-21301-5.

[8] R. Abolafia-Rosenzweig, C. He, S. McKenzie Skiles, F. Chen, and D. Gochis, "Evaluation and optimization of snow albedo scheme in noah-mp land surface model using in situ spectral observations in the colorado rockies," *Journal of Advances in Modeling Earth Systems*, vol. 14, no. 10, e2022MS003141, 2022, e2022MS003141 2022MS003141. DOI: https://doi.org/10.1029/2022MS003141. eprint: https://agupubs.onlinelibrary.wiley.com/doi/pdf/10.1029/2022MS003141. [Online]. Available: https://agupubs.onlinelibrary.wiley.com/doi/abs/10.1029/2022MS003141.

[9] C. Pohl, L. Istomina, S. Tietsche, *et al.*, "Broadband albedo of arctic sea ice from meris optical data," *The Cryosphere*, vol. 14, no. 1, pp. 165–182, 2020. DOI: 10.5194/tc-14-165-2020. [Online]. Available: https://tc.copernicus.org/articles/14/165/2020/.

[10] J. Wei, T. Ren, P. Yang, S. F. DiMarco, and E. Mlawer, "An improved ocean surface albedo computational scheme: Structure and performance," *Journal of Geophysical Research: Oceans*, vol. 126, no. 8, e2020JC016958, 2021, e2020JC016958 2020JC016958. DOI: https://doi.org/10.1029/2020JC016958. eprint: https://agupubs.onlinelibrary.wiley.com/doi/pdf/10.1029/2020JC016958. [Online]. Available: https://agupubs.onlinelibrary.wiley.com/doi/abs/10.1029/2020JC016958.

[11] C. Petrich and H. Eicken, "Overview of sea ice growth and properties," in *Sea Ice*. John Wiley Sons, Ltd, 2017, ch. 1, pp. 1–41, ISBN: 9781118778371. DOI: https://doi.org/10.1002/9781118778371.ch1. eprint: https://onlinelibrary.wiley.com/doi/

pdf/10.1002/9781118778371.ch1. [Online]. Available: https://onlinelibrary.wiley.com/doi/abs/10.1002/9781118778371.ch1.

[12] W. Huang, Z. Li, X. Liu, H. Zhao, S. Guo, and Q. Jia, "Effective thermal conductivity of reservoir freshwater ice with attention to high temperature," *Annals of Glaciology*, vol. 54, no. 62, pp. 189–195, 2013. DOI: 10.3189/2013AoG62A075.

[13] R. Stull, "Global circulation," in *Meteorology for Scientists and Engineers*, 3rd ed. Vancouver, BC, Canada, 2011, ch. 11, pp. 335–336, ISBN: 978-0-88865-178-5. [Online]. Available: https://www.eoas.ubc.ca/courses/atsc201/MSE3.html#:~:text=Stull%2C%20R.B.%2C%202011%3A%20Meteorology,%2D88865%2D178%2D5%20.

[14] M. Rantanen, A. Y. Karpechko, A. Lipponen, *et al.*, "The arctic has warmed nearly four times faster than the globe since 1979," *Communications Earth & Environment*, vol. 3, no. 1, p. 168, 2022. DOI: 10.1038/s43247-022-00498-3. [Online]. Available: https://doi.org/10.1038/s43247-022-00498-3.

[15] "Sea ice thickness and volume," DMI, Danish Meteorological Institute. (Apr. 18, 2025), [Online]. Available: https://polarportal.dk/en/sea-ice-and-icebergs/sea-ice-thickness-and-volume/ (visited on 04/18/2025).

[16] R. McGehee, *Energy balance*, Lecture in MATH 5421, University of Minnesota, Twin Cities, Feb. 18, 2025. [Online]. Available: https://www-users.cse.umn.edu/~mcgehee/Course/Math5421/slides/20250218handouts.pdf.

[17] H. Su and Y. Wang, "Using modis data to estimate sea ice thickness in the bohai sea (china) in the 2009–2010 winter," *Journal of Geophysical Research: Oceans*, vol. 117, no. C10, 2012. DOI: https://doi.org/10.1029/2012JC008251. eprint: https://agupubs.onlinelibrary.wiley.com/doi/pdf/10.1029/2012JC008251. [Online]. Available: https://agupubs.onlinelibrary.wiley.com/doi/abs/10.1029/2012JC008251.

[18] J. Walsh and C. Rackauckas, "On the budyko-sellers energy balance climate model with ice line coupling," *Discrete and Continuous Dynamical Systems - B*, vol. 20, no. 7, pp. 2187–2216, 2015, ISSN: 1531-3492. DOI: 10.3934/dcdsb.2015.20.2187. [Online]. Available: https://www.aimsciences.org/article/id/c57d9e7a-ed66-4d52-9194-85bf40aa7eb7.

[19] "Earth radius," Wikipedia.org. (Mar. 10, 2025), [Online]. Available: https://en.wikipedia.org/wiki/Earth_radius (visited on 04/14/2025).

[20] J. Selivanova, D. Iovino, and F. Cocetta, "Past and future of the arctic sea ice in high-resolution model intercomparison project (highresmip) climate models," *The Cryosphere*, vol. 18, no. 6, pp. 2739–2763, 2024. DOI: 10.5194/tc-18-2739-2024. [Online]. Available: https://tc.copernicus.org/articles/18/2739/2024/.

[21] S. Blazsek, A. Escribano, and E. Kristof, "Global, arctic, and antarctic sea ice volume predictions using score-driven threshold climate models," *Energy Economics*, vol. 134, p. 107 591, 2024, ISSN: 0140-9883. DOI: https://doi.org/10.1016/j.eneco.2024.107591. [Online]. Available: https://www.sciencedirect.com/science/article/pii/S0140988324002998.

[22] Copernicus Climate Change Service. "Esotc2023: Arctic ocean." (Jan. 1, 2024), [Online]. Available: https://climate.copernicus.eu/esotc/2023/arctic-ocean (visited on 04/12/2025).

[23] Y.-H. Kim, S.-K. Min, N. P. Gillett, D. Notz, and E. Malinina, "Observationally-constrained projections of an ice-free arctic even under a low emission scenario," *Nature Communications*, vol. 14, no. 1, 2023. DOI: 10.1038/s41467-023-38511-8. [Online]. Available: https://doi.org/10.1038/s41467-023-38511-8.

[24] K. M. Golden, L. G. Bennetts, E. Cherkaev, *et al.*, "Modeling sea ice," *Notices of the American Mathematical Society*, 2020. DOI: https://doi.org/10.1090/noti2171. [Online]. Available: https://www.ams.org/notices/202010/rnoti-p1535.pdf (visited on 04/21/2025).

[25] M. Möller, "A minimal, statistical model for the surface albedo of vestfonna ice cap, svalbard," *The Cryosphere*, vol. 6, pp. 1049–1061, 2012. DOI: 10.5194/tc-6-1049-2012. [Online]. Available: https://tc.copernicus.org/articles/6/1049/2012/.

[26] J. R. Aylmer, D. Ferreira, and D. L. Feltham, "Impact of ocean heat transport on sea ice captured by a simple energy balance model," *Communications Earth & Environment*, vol. 5, no. 1, p. 406, 2024, ISSN: 2662-4435. DOI: 10.1038/s43247-024-01565-7. [Online]. Available: https://doi.org/10.1038/s43247-024-01565-7.

[27] J. K. Shaw and J. E. Kay, "Processes controlling the seasonally varying emergence of forced arctic longwave radiation changes," *Journal of Climate*, vol. 36, no. 19, pp. 7337–7352, 2023. DOI: 10.1175/JCLI-D-23-0020.1. [Online]. Available: https://doi.org/10.1175/JCLI-D-23-0020.1.

[28] Z. Li, Q. Ding, M. Steele, and A. Schweiger, "Recent upper arctic ocean warming expedited by summertime atmospheric processes," *Nature Communications*, vol. 13, p. 362, 2022. DOI: 10.1038/s41467-022-28047-8. [Online]. Available: https://doi.org/10.1038/s41467-022-28047-8.

[29] V. V. Ivanov, V. Alexeev, N. V. Koldunov, *et al.*, "Arctic ocean heat impact on regional ice decay: A suggested positive feedback," *Journal of Physical Oceanography*, vol. 46, no. 5, pp. 1437–1456, 2016. DOI: 10.1175/JPO-D-15-0144.1. [Online]. Available: https://doi.org/10.1175/JPO-D-15-0144.1.

[30] Wikipedia. "Specific heat capacity." (Apr. 8, 2025), [Online]. Available: https://en.wikipedia.org/wiki/Specific_heat_capacity (visited on 04/20/2025).

A Investigating Linear Temperature Profile

Here, we wanted to investigate the assumption of have a linear temperature profile through the ice by solving the heat equation for the system

$$\frac{\partial T(z,t)}{\partial t} = \frac{k}{\rho c}\frac{\partial^2 T(z,t)}{\partial z^2},$$

where $c = 2.1\,\mathrm{kJ\,kg^{-1}\,K^{-1}}$ is the heat capacity of ice [30]. To solve this, I took alot of inspiration from problems solved in the course MVE 035 *Fourier Analysis* `link`. The equation was solved with the boundary conditions $T(0,t) = T_a$ and $T(h,t) = T_o$, and the initial condition $T(z,0) = (T_o - T')z/h + T'$, where T' is some arbitrary temperature. The following solution was obtained

$$T(z,t) = \sum_{n=1}^{\infty} 2\frac{T' - T_a}{n\pi}\,\sin\left(\frac{n\pi}{n}z\right)e^{-\beta t}, \text{ where } \beta = \frac{kn^2\pi^2}{\rho c h^2}.$$

The solution for $h = 4$, $T' = -7.5\,^\circ\mathrm{C}$ and $T_a = -10\,^\circ\mathrm{C}$ is given in Figure 7 for $0 < t < 30$ days, and converges to a linear function. The complete solution is available in Figure 8.

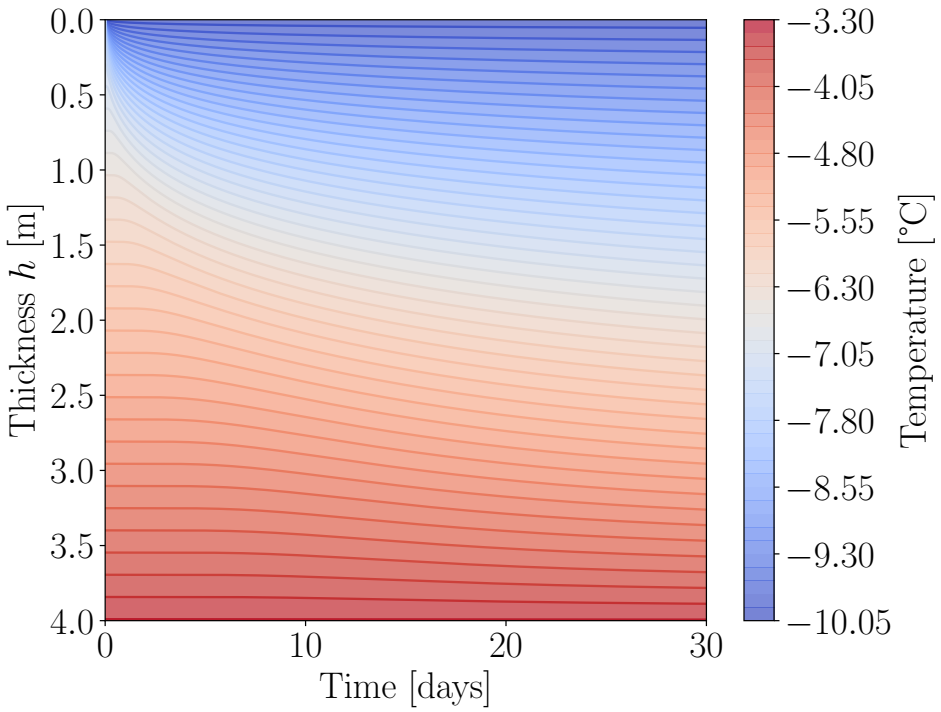

Figure 7: Solution to the heat equation with $h = 4$, $T' = -7.5\,^\circ\mathrm{C}$ and $T_a = -10\,^\circ\mathrm{C}$ for 30 days

Solving $\frac{\partial T}{\partial t} = \mathcal{D}\frac{\partial^2 T}{\partial z^2}$, with $\mathcal{D} = \frac{k}{c\rho}$ and BC: $\begin{cases} T(z=0,t) = T_a \\ T(z=h,t) = T_0 \end{cases}$; IC $T(z,t=0) = \frac{T_a - T'}{h} z + T'$

→ Splitting $T(z,t)$ into $T(z,t) = \tilde{T}(z,t) + T_s(z)$, where $\tilde{T}(z=0,t) = \tilde{T}(z=h,t) = 0$

→ Finding $T_s(z)$: $T(0,t) = \tilde{T}(0,t) + T_s(0) = T_a \Rightarrow T_s(0) = T_a$; $T(h,t) = \tilde{T}(h,t) + T_s(h) = T_0$

$\Rightarrow T_s(z) = \frac{T_0 - T_a}{h} z + T_a$ ← Steady state

→ Solving $\tilde{T}(z,t)$; ansatz: $\tilde{T}(t,z) = \tau(t) Z(z) \Rightarrow \partial_t \tau Z = \mathcal{D} \tau \partial_{zz} Z \Rightarrow \frac{\partial_t \tau}{\tau}\frac{1}{\mathcal{D}} = \frac{\partial_{zz} Z}{Z} = \lambda$ ↙ Constant.

→ Starting with Z; $\Rightarrow \Lambda^2 \equiv \lambda \Rightarrow \partial_{zz} Z - \Lambda^2 Z = 0 \Rightarrow \begin{cases} (i)\ Z(z) = Ae^{-\Lambda z} + Be^{\Lambda z} \\ (ii)\ Z(z) = \alpha \sin(\Lambda z) + \beta \cos(\Lambda z) \end{cases}$

(i) BC $Z(0) = 0 = A + B \Rightarrow A = -B$; $Z(h) = 0 = Ae^{\Lambda h} + Be^{-\Lambda h} = A(e^{\Lambda h} - e^{-\Lambda h}) = 2A\underbrace{\sinh(\Lambda h)}_{\neq 0, h, \Lambda \neq 0} = 0 \Rightarrow A = 0$

(ii) BC $Z(0) = 0 = \alpha \cdot 0 + \beta \cdot 1 \Rightarrow \beta = 0$; $Z(h) = 0 = \alpha \sin(\Lambda h) \Rightarrow \Lambda_n = \frac{n\pi}{h} \Rightarrow \lambda_n = n^2\pi^2/h^2$

$\Rightarrow Z_n(z) = \alpha \sin(n\pi k)$

→ Time part: $\partial_t \tau_n = \mathcal{D}\lambda_n \tau_n \Rightarrow \tau_n(t) = \tau_0 e^{\mathcal{D}\lambda_n t} = \tau_0 e^{-\mathcal{D}t(n\pi/h)^2}$

→ Solution: $T(z,t) = \sum_{n=1}^{\infty} \tau_n(t) Z_n(z) + T_s(z) \overset{\tau_0 \alpha = \alpha_n}{=} \sum_{n=1}^{\infty} e^{-\mathcal{D}t(n\pi/h)^2} \alpha_n \sin(\frac{n\pi}{h} z) + \left(\frac{T_0 - T_a}{h} z + T_a\right)$

→ Initial condition: $T(z,0) = \frac{T_a - T'}{h} z + T' = \sum_{n=1}^{\infty} \alpha_n \sin(\frac{n\pi}{h} z) + \left(\frac{T_0 - T_a}{h} z + T_a\right) \Leftrightarrow \sum_{n=1}^{\infty} \alpha_n \sin(\frac{n\pi}{h} z) = \frac{T_a - T_0}{h} z - T_a + \frac{T_a - T'}{h} z + T' = \frac{T_a - T'}{h} z + T' - T_a$

→ Finding α_n with Fourier series: $\alpha_n = \left\langle \frac{T_a - T'}{h} z + (T' - T_a),\ \sin(\frac{n\pi}{h} z) \right\rangle \Big/ \|\sin(\frac{n\pi}{h} z)\|$; $\|\sin(\frac{n\pi}{h} z)\| = \int_0^h \sin^2(\frac{n\pi}{h} z)\, dz = \ldots = \frac{h}{2}$

$\Rightarrow \frac{2}{h}\left\langle \frac{T_a - T'}{h} z + (T' - T_a),\ \sin(\frac{n\pi}{h} z) \right\rangle = \frac{2}{h}\left[\int_0^h \frac{T_a - T'}{h} z \sin(\frac{n\pi}{h} z)\, dz + \int_0^h (T' - T_a)\sin(\frac{n\pi}{h} z)\, dz\right] =$

$= \frac{2}{h}\left[\frac{T_a - T'}{h}\left(\left[-\frac{h}{n\pi} z \cos(\frac{n\pi}{h} z)\right]_0^h + \int_0^h \frac{h}{n\pi} \cos(\frac{n\pi}{h} z)\, dz\right) + \left[(T' - T_a)\frac{h}{n\pi}\cos(\frac{n\pi}{h} z)\right]_0^h\right] = \frac{2(T_a - T')}{h^2}\frac{h}{n\pi}\left(-h\cos(n\pi)\right) + \frac{2(T' - T_a)}{h}\frac{h}{n\pi}\left(1 - \cos(n\pi)\right)$ (the $\int \cos$ term $= 0$)

$= \frac{2}{n\pi}\left[(T' - T_a)\cos(n\pi) + (T' - T_a)(1 - \cos(n\pi))\right] = \frac{2}{n\pi}(T' - T_a)$

In conclusion: $T(z,t) = \sum_{n=1}^{\infty} \alpha_n \sin(\frac{n\pi}{h} z)\, e^{-\mathcal{D}t(n\pi/h)^2} = \sum_{n=1}^{\infty} \frac{2}{n\pi}(T' - T_a)\sin(\frac{n\pi}{h} z)\, e^{-\mathcal{D}t(n\pi/h)^2}$

Figure 8: Full solution to the heat equation with the given boundary and initial conditions.